Feasey, W. F. F., Austin, J.M., Hornung, H. G.: Characterising the Step Response of a Static Pressure Probe. California Institute of Technology, Pasadena, CA, USA. Presented at the 35th International Symposium on Shock Waves (ISSW35), Brisbane, Australia, 05-14 July 2025.

Characterising the Step Response of a Static Pressure Probe

William F. F. Feasey[1], Joanna M. Austin[1], and Hans G. Hornung[1]

California Institute of Technology, 1200 E California Blvd, Pasadena, 91125, U.S.A.
w.feasey@caltech.edu

Abstract. We examine the transient rise in static pressure in response to the passage of a planar shock wave as measured by Caltech's V3 probe. The V3 was designed as a small-scale static pressure probe for routine freestream characterisation in situ with models in the T5 free-piston shock tunnel. A two-regime, choked-unchoked model is tested via an extensive experimental shocktube campaign. Freestream conditions spanned $\mathrm{Re}_\infty = (0.08{-}2.56){\times}10^6$ m^{-1}, $\mathrm{M}_\infty = 1.2{-}3.5$, $p_\infty = 4{-}33$ kPa, with helium, air, carbon dioxide, and combinations thereof, used as test gases in order to explore Reynolds number and sound speed scaling. Navier-Stokes simulations were performed of post-shock flow into the cavity housing the pressure sensor. Functional relationships relating rise time during choked conditions to both an acoustic time scale and the freestream Reynolds number were identified and compared with experimental and computational correlation fits.

Keywords: hypersonic ground testing, hypervelocity, shock tube, static pressure, cavity rise time

1 Introduction

Characterization of freestream quantities in hypersonic facilities is critical for operation monitoring and interpretation of test results. In impulse facilities capable of replicating high-speed flow, the temporal response of sensors is particularly important. A series of three, high-frequency static pressure probes have been constructed at Caltech for the purpose of providing time-resolved measurements in the T5 reflected shock tunnel [1,2], with the V3 model, considered in this work, specifically designed for routine use with models in place. Satisfactory measurements of the test-time static pressure have been obtained, exhibiting agreement with shot-by-shot simulations of the T5 freestream [3] and also, more recently, implicit static pressure calculations using tunable diode laser absorption spectroscopy (TDLAS) data [4]. However, there remains some uncertainty as to the temporal response of the static probe and the design optimization to capture the transient nozzle startup process [2].

The design of these static pressure probes used in this study is inspired by Behrens [5] and consists of a needle-like probe with four opposing orifices, allowing flow access to the transducer. Alternative probe geometries have been

developed where reduced sensitivity to angle of attack [6] and enhanced flow recovery [7] are of heightened importance. Studies of cavity domain inflow have been made both computationally and experimentally, with particular emphasis directed towards describing pressure fluctuations and minimising acoustic resonance with geometry optimisation [8,9].

In this work, we examine the filling mechanism of the probe cavity subject to transverse, post-shock flow. We test over a wide freestream parameter space via experiments and numerical simulations, the latter with a particular emphasis on the role of inflowing pathlines and streamwise inhomogeneity across the orifices.

2 Theoretical Considerations

To a first approximation, the filling mechanism between the probe exterior and internal cavity can be demarcated into a period of choked flow, followed by pressure-driven, unchoked flow. The transition between the two is defined by the critical point, $p_c = p(t_c)$. We take this two-regime approach as our starting point and systematically explore its limitations. The following formulation closely follows that of Hornung [10] and for brevity's sake we just state the main results here. The piecewise equation for pressure rise within the cavity is given by:

$$\frac{p(t)}{p_e} = \begin{cases} B(\gamma)\left(\frac{t}{\tau}\right)^{\gamma} & t < t_c \\ 1 - \left(1 - \frac{p_c}{p_e}\right) e^{-C(\gamma)\frac{t-t_c}{\tau}} & t > t_c, \end{cases} \tag{1}$$

where an acoustic time scale has been introduced: $\tau = V/(a_e A)$ relating cavity volume (V), total inlet area (A) and local sound speed external to the orifice (a_e). $B(\gamma)$ and $C(\gamma)$ denote weakly varying functions of the specific heat ratio (γ), defined through imposing $\mathcal{C}^0$ and $\mathcal{C}^1$ continuity about the critical point (t_c, p_c). The orifice flow is assumed to be both adiabatic and frictionless in deriving Eq. 1.

A further assumption is streamwise and spanwise homogeneity of the flow through the orifice. Of the two, we expect streamwise non-uniformities to be the most extreme. Indeed it becomes apparent from the cavity simulations (sec. 4.2) that there is significant variation in the streamwise mass flux. In the simplified analysis above, the reservoir state, $\{p_e, a_e\}$, is initially at rest; however, in reality, the initial set of particle pathlines filling the cavity are defined by the boundary layer edge state, $\{p_e, a_e, U_e\}$, external to the orifice. Immediately following the transient shock the pathlines undergo a rapid expansion around the leading edge of the orifice. Any streamwise variation in mass flow is therefore driven by the differing isentropic paths taken by each entrained pathline. We relax the choked assumption of Eq. 1, and consider a more general pressure rise along pathlines, while maintaining our isentropic assumption:

$$\frac{\mathrm{d}m}{\mathrm{d}t} = \rho \mathbf{u} \cdot \mathbf{A} \quad \& \quad \frac{u_y}{a_e} = \frac{u_y}{a}\frac{a}{a_e} = \frac{\mathrm{M}_y}{\sqrt{1+\frac{\gamma-1}{2}\mathrm{M}^2}}$$
$$\implies \frac{1}{p}\frac{\mathrm{d}p}{\mathrm{d}t} = \gamma \underbrace{\frac{\mathrm{M}_y}{\sqrt{1+\frac{\gamma-1}{2}\mathrm{M}^2}}}_{\text{supersonic term}} \underbrace{\frac{a_e A}{V}}_{1/\tau} \tag{2}$$

where u_y and M_y are the velocity and Mach number parallel to the orifice axis. Eq. 2 relates the pressure rise along a pathline in terms of the acoustic time scale, but is also driven by a supersonic term[1], describing departure from choked flow. This modification allows us to make two predictions: 1. A larger Re_∞ produces a thinner boundary layer and as such, the average velocity along the entrained pathlines is higher, thus filling the probe at a faster rate; 2. The 'supersonic' term in Eq. 2 asymptotes for larger Mach numbers $\rightarrow \sqrt{\frac{2}{\gamma-1}}\frac{\mathrm{M}_y}{\mathrm{M}}$ and hence, the impact of larger Re_∞ will diminish as the supersonic term is driven towards a constant.

3 Experimental Work

3.1 Static Probe Design

The static probe implemented in this work is referred to, in-house, as the V3 static probe. Designs of previous probes, particularly pertaining to reduction in cavity volume, are reported in Yu et al. [1,2]. A cross-section of the hypodermic tube cavity in front of the Kulite transducer is shown in Fig. 1, with the dimensions of each labelled cavity feature shown in Table 1. Four circular, straight-cut orifices connect the external flow to an approximately cylindrical cavity. The V3 design places the Kulite face extremely close to the trailing edge of the orifice, while the leading edge is flush with an epoxy-steel wool mixture to fill the opposing void. Together these two design choices minimise the effective cavity volume, without compromising on inlet area.

3.2 Instrumentation

The Kulite XCS-062 data are collected at a 2.5 MHz sampling rate, using a National Instruments PXI-1031 data acquisition system, having been amplified with a Vishay 2310B signal conditioner. A voltage-pressure calibration curve was produced before each test: during evacuation of the facility, the voltage signals from both the Kulite and an additional Baratron Capacitance Manometer, were recorded at 30Hz over a pressure range spanning at least $p_\infty \pm 50\%$.

[1] Note any *a priori* prediction of the streamwise Mach number distribution through the orifice is complicated by the 3D geometry. However, in evaluating $\{\mathrm{M}_y, M\}$ from simulations, we can see the usefulness of Eq. 2.

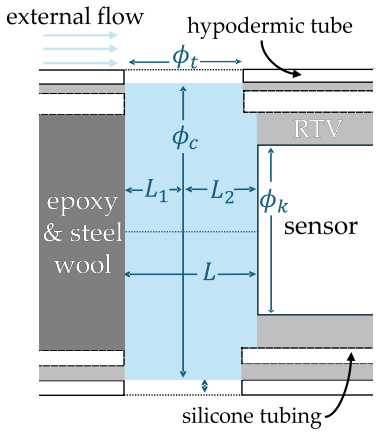

Fig. 1: Schematic of internal cavity dimensions of V3 probe.

Table 1: Geometric dimensions of the static probe cavity.

	Description	(mm)
ϕ_t	tap diameter	1.52
ϕ_k	Kulite diameter	1.59
ϕ_c	cavity diameter	3.68
L_1	epoxy setback	0.76
L_2	Kulite setback	0.82
L	cavity length	1.59
t_{hyp}	hypodermic tube thickness	0.36
A	tap entrance area, $4\pi L_1^2$	7.24 mm^2
V	cavity volume, $\frac{1}{4}\pi\phi_c^2$	16.9 mm^3

3.3 HET Facility

The Hypervelocity Expansion Tube (HET) is an impulse facility comprising of three sections: the driver (1.22m), driven (3.96m) and expansion (3.96m) sections of constant internal diameter of 152 mm [11]. In these experiments, the secondary diaphragm between driven and expansion sections was omitted, and the facility was operated in conventional shock tube configuration.

3.4 Experimental Results

Characterising Rise Time Two examples of experimental pressure traces are shown in Fig. 2. Significant oscillations were observed around the Kulite resonant frequency (period $\approx 6.7\mu$s) in each pressure trace, complicating the quantification of any rise time metric. The Kulite diaphragm can be approximated as second-order system and as such, both signal gain and phase lag become non-negligible in this regime. To make quantitive comparisons of pressure rise between tests, both a minimal-bias filter and robust rise time metric were developed: a combined lowpass (40kHz), moving-mean (15 point window) filter was applied to all data collected and is shown in Fig. 2. The two filtering parameters were optimised to minimise bias across the range of conditions tested. The error associated with this filtering procedure was the main source of uncertainty in reported rise time metric and is estimated to be $\sim 8\%$. The rise metric selected was the *intercept time*, t_i: the point of maximum gradient in the filtered signal was identified as the critical time, t_c, and the local gradient was extrapolated up to the steady, test time pressure, $p = p_{tt}$, intersecting at a time, t_i.

Sound Speed Dependence We ran experiments to probe the role of freestream sound speed, varying $a_\infty = 1 - 2$ km/s, at a constant unit Reynolds num-

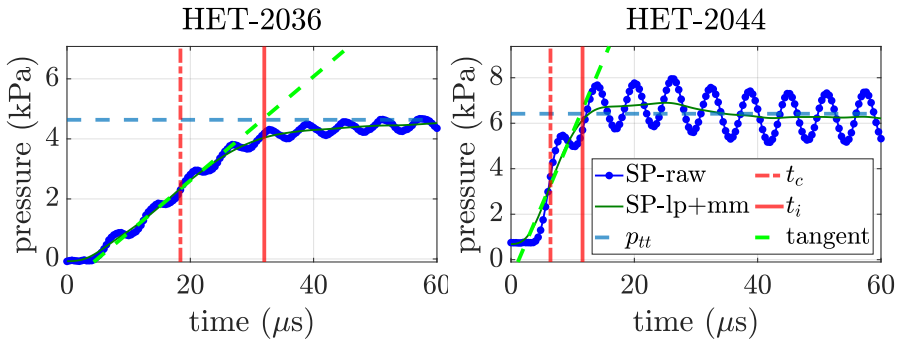

Fig. 2: Two examples of experimentally measured pressure rises. Both the raw pressure trace (dotted blue) and the filtered signal (dark green) are shown, in addition to the asymptotic test time pressure (p_{tt}). Critical time (red dashed), intercept time (red solid) and the critical tangent (dashed lime green) are also overlaid.

ber, $\mathrm{Re}_\infty \approx 1.6 \times 10^5$ m^{-1} (coefficient of variation = 1.5%). Fig. 3 shows the recorded intercept times plotted against theoretical freestream sound speed values. Both a theoretically motivated inverse sound speed, and generalised power law, $t_i = \beta a_e^{-\alpha}$ relationship were compared and excellent fits were obtained: $\alpha = 1$ ($\mathrm{R}^2 = 0.991$) and $\alpha = 1.06$ ($\mathrm{R}^2 = 0.996$), respectively.

Reynolds number dependence Expanding the span of experimental conditions tested, it was found the sound speed alone was insufficient to fully collapse the data, deviating from the simple choked-unchoked model. Eq. 2 suggests the fractional pressure increase should be linear in γ and $1/\tau$, thus motivating the normalised rise time variable: $t' = t_i\,(\tau/\gamma)^{-1} \equiv t_i(\gamma a_e A)/V$.

A systematic correlation analysis was performed to determine which dimensionless variables best fit the data and a generalised power law consisting of reduced time, t', and Reynolds number, Re, proved the most fruitful. No length scales were independently varied in the course of this work and so an arbitrary Reynolds number was defined, contingent upon the orifice tap diameter, $\mathrm{Re} = \rho_\infty U_\infty \phi_t / \mu_\infty$. The resulting reduced data is plotted in Fig. 3b, and the fit $t' \propto \mathrm{Re}^{-0.43}$ ($\mathrm{R}^2 = 0.94$) shows excellent agreement over a wide range of freestream conditions. The diminishing impact of Re is also in accordance with the intuition developed in section 2.

4 Numerical Study

4.1 Computational Codes Used

LETS is a gas dynamic simulation tool used to conduct fast parameter sweeps of the HET facility operating envelope, and design theoretical freestream conditions

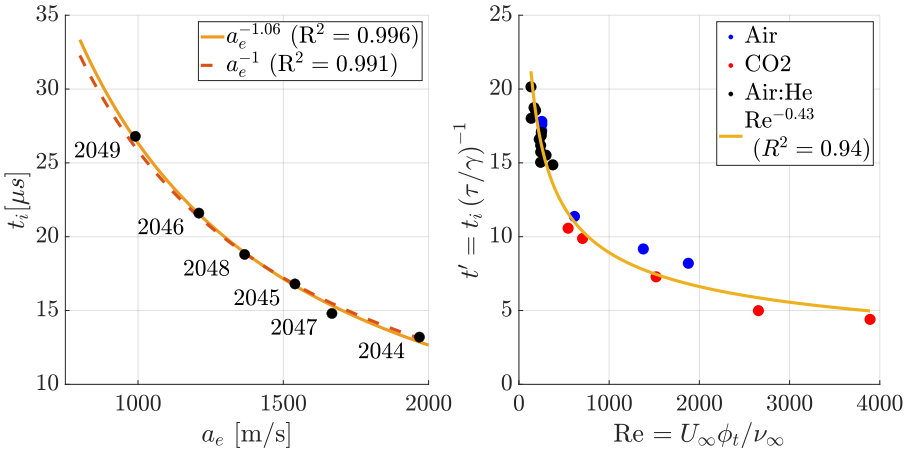

Fig. 3: a) Intercept time against sound speed, for constant $\mathrm{Re}_\infty \approx 1.6 \times 10^5$ m^{-1} b)Sound speed normalised rise time vs Reynolds number across all experiments. Generalised power law fit is shown in yellow.

[12]. A variety of test gas compositions were selected to obtain a continuous spectrum of $\{a_\infty, \gamma, \mathrm{Re}_\infty\}$. Navier-Stokes simulations of the post-transmitted shock flow, both exterior to the probe and into the cavity, were carried out using `Eilmer4` [13]. Thermally perfect, non-reacting gas was assumed throughout. All simulations were fully viscous, assuming no-slip boundary conditions at each solid surface. Cell clustering was employed proximal to physical walls to ensure all boundary layers were adequately captured along the external surface of the model.

4.2 Simulation Results

External Pressure Recovery Numerous inviscid and viscous computational studies have examined the freestream pressure recovery around a static pressure probe, particular focussing on high Mach number cases [14,1,7]. An axisymmetric grid was constructed to evaluate both the pressure recovery of the freestream and the induced pressure across the boundary layer. The computational domain spanned $N_x \times N_y = 280 \times 200$. Fig. 4 shows an example flow field established around the probe (HET2031 freestream) as well as the static pressure along the surface of the probe (p_e) for various Mach numbers. Across the span of our experiment campaign, the pressure had fully recovered to the freestream value at the orifice location.

Simulation of Cavity Flow Formation A 2D, axisymmetric simulation was constructed to elucidate the filling mechanism that results in the formation of cavity flow. The cavity volume is matched to that of the real probe model and

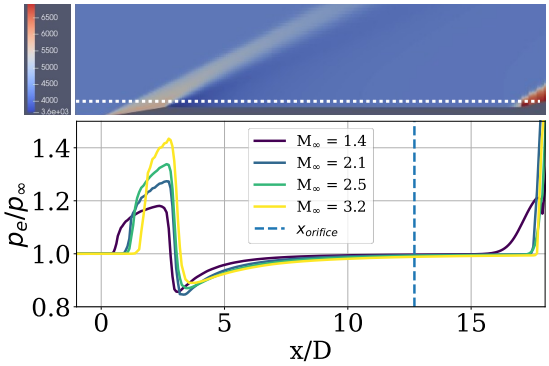

Fig. 4: Example flow field established around the static probe (flow conditions from HET2031). Pressure contours are in Pa and the pressure external to the probe (p_e) is plotted along the horizontal, dashed white line, for differing M_∞.

the effective filling area of uniform cylindrical inlet ring is also consistent. Fig. 5 shows three snapshots of the cavity pressure field over a simulation interval of 25μs. The volume-weighted average cavity pressure and trailing-surface pressure are plotted over the simulation duration. Also plotted is the streamwise-averaged mass flux through the orifice, normalised with respect to the theoretical sonic mass flux, $\dot{m}^* = \rho_e^* a_e^*$. Initially, the shock traverses the orifice in $\sim 0.5\mu$s and impinges on the trailing edge of the orifice, locally stagnating the flow. The post-shock flow expands around the leading edge causing a partial acceleration followed by a rapid deceleration as the supersonic flow is contracted through the trailing section of the orifice. Frame B shows the establishment of steady, choked flow. The modified converging-diverging flow field is highlighted by the sonic isolines (green) appearing at both the inlet and outlet of the orifice. Choked flow is quantitatively reflected by fast rises in cavity pressure and a constant orifice mass flux. Once the orifice exit pressure exceeds the critical pressure, the flow un-chokes and the orifice flow field becomes dominated by the primary recirculation vortex (Frame C). The net entrainment of flux into the cavity is drastically reduced and the pressure rise decelerates significantly.

Role of Reynolds Number To better understand the physical means by which Re affects the choked regime, a series of 2D simulations were conducted. Freestream sound speed was held approximately constant ($a_\infty = 1480 - 1487$ m/s), while freestream Reynolds number was varied over an order of magnitude ($\mathrm{Re}_\infty = 5 \times 10^4 - 4 \times 10^5$ m^{-1}). Deviations from sonic-limited choked flow, are characterised by the supersonic quantity defined in Eq. 2, and plotted for each case as a function of time in Fig. 6b. The highest Reynolds number case (HETa2) attains the largest magnitude of inflow velocity, as is expected by our modified theory, and the breakdown of choked flow occurs earlier. The modified inflow is reflected in the normalised intercept times, calculated in identical fashion to

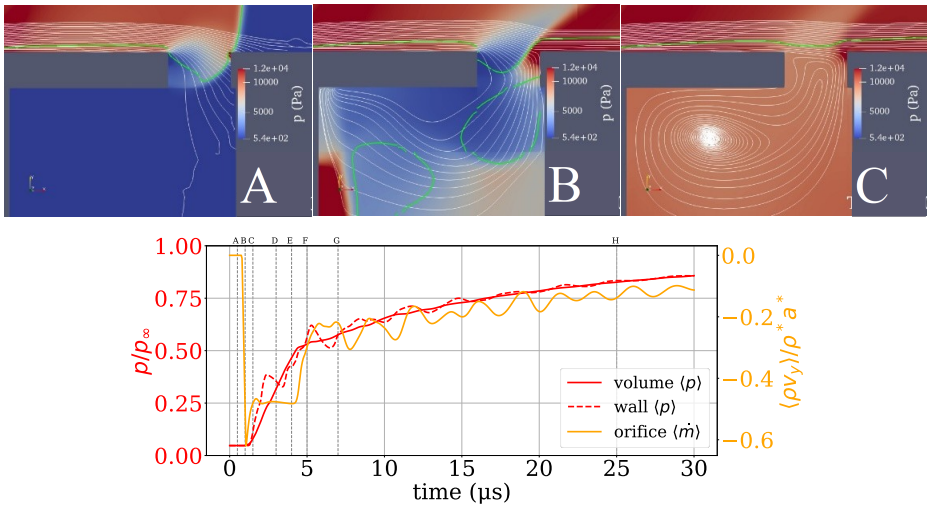

Fig. 5: Three snapshots from 2D axisymmetric simulations showing the pressure rise inside the cavity and incoming pathlines in white. Contours of sonic Mach number $\mathrm{M} := |\mathbf{u}|/a = 1$, are shown as green lines. Cavity pressure averaged over entire volume (solid red), effective Kulite face (dashed red) and normalised mass flux through orifice (orange) are plotted. Grey dotted line indicate the time instances of snapshots

that used in the experimental methodology. Higher Re clearly decreases intercept time, with an optimal power fit found to be $t' \propto \mathrm{Re}^{-0.33}$ ($\mathrm{R}^2 = 0.97$). The dependency is marginally weaker than that found experimentally ($t' \propto \mathrm{Re}^{-0.43}$) most likely a by-product of these being 2D simulations, and thus not accounting for spanwise inflow reduction.

Discussion of Unchoked Regime Much of the preceding analysis has focussed on the period of choked flow, given that it is responsible for the large initial pressure rise and can be modelled with relatively simple ideas of quasi-1D gas dynamics. The unchoked regime is greatly affected by the cavity vortex extending in to the orifice itself, drastically reducing the net inflow. Some progress was made in constructing a full 3D simulation, adhering to the true dimensions of the physical static probe. The main limitation with the 3D simulations was the strong expansion around the leading lip of the orifice proving to be numerically unstable. Initial 3D simulations suggested a fill completion time ($p = 0.99 p_{tt}$) of $t_{99} \approx 15\tau$, four times longer than that predicted by the 1D model (Eq. 1).

5 Conclusions

The response of the V3 static pressure probe to a step change (planar shock wave) has been explored in order to assist interpretation of temporal results for

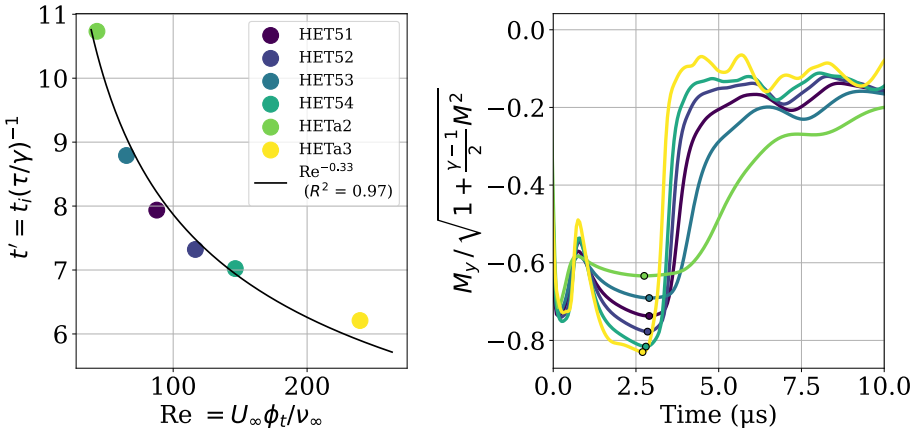

Fig. 6: 2D-axissymetric cavity simulations: a) intercept time normalised by τ/γ plotted against Reynolds number. A generalised power law fit is overlaid in black. All cases set $a_\infty \approx 1.5$km/s with HET51-54 corresponding to experimentally tested freestream conditions and HETa2-3 additional numerical conditions; b) the spanwise-averaged supersonic parameter plotted against time.

T5 experiments, with comparisons to theoretical and numerical modelling. Our conclusions are summarised here:

1. A two-regime, choked-unchoked model qualitatively captures the dynamic response of a static pressure probe responding to post-shock flow.
2. The experimental static pressure response exhibited sensor resonance, partially obscuring the rise characteristics; however the intercept time, t_i, was identified as a robust measure of initial pressure rise during the choked phase.
3. Experiments suggest intercept time varies inversely with characteristic acoustic time scale and a weak Reynolds number dependence is also identified ($t_i \propto \tau \cdot \mathrm{Re}^{-0.43}$).
4. Both 2D and 3D simulations of the cavity flow dynamics are computed, and a similar scaling is observed ($t_i \propto \tau \cdot \mathrm{Re}^{-0.33}$).
5. The cavity aspect ratio of the V3 probe is identified as being beneficial: the Kulite face is exposed to the dynamic pressure of the orifice inflow, thus raising pressure faster than might be expected during the choked regime.
6. During the unchoked regime, the resulting recirculation vortex increases the total time to steady cavity pressure: $t_{99} \sim \mathcal{O}(30 - 50\mu\mathrm{s})$.

Acknowledgements

The authors would like to thank Dr. Wesley Yu specifically for introducing the project and Noel Esparza-Duran for his machining mastery. This work was supported in part by the Air Force Office of Scientific Research through Award

No. FA9550-23-1-0446 with Drs. Mike Berman and Amanda Chou as program officers.

References

1. Wesley M. Yu et al. Freestream static pressure measurements in the t5 reflected shock tunnel. *AIAA SciTech Forum*, 2022.
2. Wesley M. Yu et al. High-frequency static pressure measurements in the t5 reflected shock tunnel. Number AIAA 2024-2884, January 2024.
3. H. G. Hornung. T5 nozzle computation with specified throat-condition history. Technical report, Jul 2023. Accessed: 2024-12-14.
4. Julian J. Girard et al. Measurements of reflected shock tunnel freestream nitric oxide temperatures and partial pressure. *AIAA Journal*, 59(12):5266–5275, 2021.
5. Wilhelm Behrens. Viscous interaction effects on a static pressure probe at m equals 6. *AIAA Journal*, 1(12):2864–2866, 1963.
6. S. Z. Pinckney. A short static-pressure probe design for supersonic flow. Nasa technical note, NASA Langley Research Center, Hampton, VA, 1975.
7. Guillaume Grossir et al. Free-stream static pressure measurements in the longshot hypersonic wind tunnel. *Experiments in Fluids*, 57(1):64, 2016.
8. A. R. Porro. Pressure probe designs for dynamic pressure measurements in a supersonic flow field. In *ICIASF 2001 Record*, pages 417–426, 2001.
9. Chao Wang et al. The mechanism of how a cavity affects the fluctuating pressure measurement results of a static pressure probe. *Dynamics*, 3(4):777–790, 2025.
10. H. Hornung. Response of pressure tap. Internal report, California Institute of Technology, 2004.
11. A. Dufrene et al. Design and characterization of a hypervelocity expansion tube facility. *Journal of Propulsion and Power*, 23(6):1128–1135, 2007.
12. Joel M. Lawson et al. Design of conventional and detonation-driven hypervelocity expansion tubes. Number AIAA 2018-3566, June 2018.
13. Nicholas N. Gibbons et al. Eilmer: An open-source multi-physics hypersonic flow solver. *Computer Physics Communications*, 282:108551, 2023.
14. S. Karl. *Numerical Investigation of a Generic Scramjet Configuration.* Phd dissertation, Technical University of Dresden, 2011.